Solid Earth Discuss., 4, 823–850, 2012
www.solid-earth-discuss.net/4/823/2012/
doi:10.5194/sed-4-823-2012

Solid Earth Discussions

Segmentation of the Izu-Bonin and Mariana plates based on the analysis of the Benioff seismicity distribution and regional tomography results

K. Jaxybulatov, I. Koulakov, and N. L. Dobretsov

Institute of Petroleum Geology and Geophysics SB RAS, Prospekt Koptyuga, 3, 630090, Novosibirsk, Russia

Received: 7 June 2012 – Accepted: 18 June 2012 – Published: 5 July 2012

Correspondence to: K. Jaxybulatov (jaxybulatov@gmail.com)

Published by Copernicus Publications on behalf of the European Geosciences Union.

Abstract

We present a new model of P- and S-velocity anomalies in the mantle down to 1300 km depth beneath the Izu-Bonin and Mariana (IBM) arcs. This model is derived based on tomographic inversion of global travel time data from the revised ISC catalogue. The results of inversion are thoroughly verified using a series of different tests. The obtained model is generally consistent with previous studies of different authors. We also present the distribution of relocated deep events projected to the vertical surface along the IBM arc. Unexpectedly, the seismicity form elongated vertical clusters instead of horizontal zones indicating phase transitions in the slab. We propose that these vertical seismicity zones mark zones of intense deformation and boundaries between semi-autonomous segments of the subducting plate. The P- and S-seismic tomography models consistently display the slab as prominent high-velocity anomalies coinciding with the distribution of deep seismicity. Based on joint consideration of the tomography results and the seismicity distribution we propose a scenario of the subduction evolution in the IBM zone during the recent time. We can distinguish at least four segments which subduct differently. The northernmost segment of the Izu-Bonin arc has the gentlest angle of dipping which is explained by backward displacement of the trench. In the second segment, the trench stayed at the same location, and we observe the accumulation of the slab material in the transition zone and its further descending to the lower mantle. In third segment, the trench is moving forward that causes steepening of the slab. Finally, for the Mariana segment, despite the backward displacement of the arc, the subducting slab is nearly vertical. We propose that it might be due to the high density of the slab which is responsible for turning any inclined subduction to the vertical position. Between the Izu-Bonin and Mariana arcs we clearly observe a gap which is traced down to about 400 km depth.

SED
4, 823–850, 2012

1 Introduction

Subduction zones are the most spectacular geological objects where intensive geodynamic processes occur. Strong mechanical deformations and complex geochemical processes in subduction zones are responsible for the diversity of various geological structures observed on the surface. Investigating the links between surface geology and processes in the subducting slab is an actual problem that involves many specialists from different fields of geology and geophysics (e.g. Dobretsov et al., 2012). The general concept of subduction is confirmed by a number of different data and accepted by most specialists in the world. However, the details of this process are the subject of intensive debates. In particular, representation of the subduction zones as a two-dimensional conveyer-type process appears to be in most cases oversimplified and it does not explain many important phenomena. For example, the distribution of deep seismicity, arc volcanism properties and dipping regimes of slabs may abruptly change along the subduction. There are many open questions related to subduction zones, and to answer them, new robust and reliable data on the deep structure are still required.

Izu-Bonin-Mariana (IBM) arc is located in the western Pacific (Fig. 1). The arc length is more than 2800 km and it extends from north to south, from Tokyo Bay to Guam. This intraoceanic convergent zone is the result of a multi-stage subduction of the Pacific plate beneath the Philippine plate. There are the remnants of ancient arcs, such as the Kyushu-Palau Ridge with the age of volcanism 37–25 million yr (Peive, 1980; Hilde et al., 1983), the West Mariana Ridge with the age of volcanism 23–10 million yr and Bonin Ridge and the dead zones of extension, such as the Shikoku Basin, Parece Vela Basin (extension age 25–15 Ma) and the West Philippine Basin (with the age of oceanic plate 100–150 Ma). In the active back-arc basin of Mariana Trough, the extension began about 3 million yr ago (Peive, 1980; Fig. 1). This process caused oceanward displacement of the Mariana trench and forming a loop shaped arc. The age of the Pacific Plate varies along the IBM arc from 146 Ma in the northern segments

SED
4, 823–850, 2012

to 155 Ma at the Mariana trench (e.g. Müller et al., 1997). The rate of the Pacific plate subduction in respect to the Philippine Plate is 4.9 and 4.0 cm yr^{-1} in the northern and southern segments of the Izu-Bonin arcs; in the Mariana arc it changes from 2.8 to 1.6 cm yr^{-1} when moving southward (DeMets et al., 1994, 2010). The rate of eastward displacement of the Mariana trench is about 2 cm yr^{-1} (DeMets et al., 2010). This area is also remarkable as a place of the deepest point of the Earth surface which is located in the Mariana Trench.

There are more than 20 volcanic islands along the Izu-Bonin arc and more than 70 along the Mariana arc (Baker et al., 2008). Most of the volcanoes along the IBM arc are submarine. Figure 1 shows the location of the volcanoes and tectonic units of different ages. The volcanoes of the IBM arc are generally characterized by low dacite and andesite content (Kelemen et al., 2004) and a frequent occurrence of the boninite series, which were first discovered and described in this region (Petersen, 1891; Crawford et al., 1981). These composition features make the IBM volcanoes particular compared to other subduction zones of the world.

The structure of the subducting slab in the IBM area have been investigated in a number of different studies. The first information on the shape of the subduction zone was derived from the analysis of depth distribution of seismicity in the Benioff zone (e.g. Katsumata and Sykes, 1969; Engdahl et al., 1998). More details on the slab structure beneath the IBM arc were found in a number of seismic models on the global (e.g. Bijwaard et al., 1998) and regional scales (Widiyantoro, 1999; Widiyantoro and van der Hilst, 1996; Gorbatov et al., 2003; Miller et al., 2004, 2005, 2006a) mostly constructed by tomographic inversion of body wave travel times. These studies reveal generally consistent information on the shape of the subducting slab, but in details they appear to be considerably different. For example, the fact of penetration of the slab into the lower mantle is still actively debated, and the behavior of the slab in the contact zone between Izu-Bonin to the Mariana segments is not clear yet. The inconsistencies between different models are partly due to the fact that seismic tomography based on noisy earthquake data is not a perfect tool; often processing of same data by different

SED
4, 823–850, 2012

authors leads to considerably different results. Therefore any attempt to compute a new model using independent approaches is an important step to corroborate the existing information and it is greatly appreciated by the scientific community.

The behavior of the slab beneath the IBM arc has been actively discussed in a series of papers by Miller et al. (2004, 2005, 2006a, b). They reconstructed the position of the trench in the last 30 Ma and explained the variable shapes of the slab along the IBM arc by the mutual displacements of the trench and the oceanic plate. The bend around the contact zone between Izu-Bonin and Mariana arc is explained by presence of highly buoyant segment in the incoming plate with large igneous Ogasawara Plateau. At the same time, we are not satisfied by their explanation of the vertical shape of the Mariana slab by forward displacement of the trench (Fig. 10 in Miller et al., 2006b). We did not find in the literature any evidence of forward displacement of the Mariana segment of the trench (Seno and Maruyama, 1984; Seno et al., 1993; Hall et al., 1995a, b; Hall, 2002); just opposite, most authors show the backward displacement. In the discussion session we will propose an alternative point of view based on our tomography results.

In this study we present a new seismic model of the mantle seismic structure down to 1300 km depth beneath the IBM arc. For this model, we use more recent version of the ISC catalogue compared to the previous studies which contains considerably larger data amount. It is important that we use our own algorithm which has some particularities compared to the previous studies. We present several tests which demonstrate the limitations of the resolution and support the robustness of the derived structures. In this paper we compare our model with the existing ones and discuss possible geodynamical interpretation of the results.

2 Data processing and algorithm

In this study we use the travel times of P- and S-waves from the International Seismological Centre (ISC) for the time period from 1964 to 2007. The advantage of the

SED
4, 823–850, 2012

ISC dataset is a long registration period and the global data coverage which cannot be achieved by any regional network. At the same time, the data quality in the initial ISC catalogue is low. The reported coordinates of events are strongly biased due to outdated location algorithm and a big number of outliers in the data. Therefore, before using for tomographic inversion, this catalogue should be reprocessed. Most of scientists use a revised EHB catalogue which was created from careful refining of the ISC data by Engdahl et al. (1998). For our studies, we perform our own revision in which the rejection of outliers and relocation of sources were performed using the algorithm described in (Koulakov and Sobolev, 2006). This revised catalogue has been constructed based on the 1D reference model AK 135 (Kennett at al., 1995) and takes into account the ellipticity of the Earth and variable crustal thickness according to the global model CRUST2.0 (Bassin et al., 2000). Our approach is less conservative compared to one used by Engdahl et al. (1998), and it keeps more data, which is favorable for tomographic inversion.

Regional tomographic inversion in this study is based on the approach proposed by Koulakov et al. (2002). In later works, this algorithm was modified and used to study the upper mantle structure beneath some regions (see, for example, Koulakov et al., 2009, 2011; Koulakov, 2011). This tomographic inversion algorithm is based on the linearized approach which imply that all calculations are performed on the basis of rays constructed in one-dimensional model AK135 (Kennett at al., 1995). It should be noted that there is no theoretical difficulty of using a nonlinear algorithm with a three-dimensional ray tracing (for example, as used in the LOTOS code by Koulakov, 2009). However, we do not believe that implying the iterative non-linear inversions would bring principal changes in the results. First, the recovered amplitudes of anomalies in the upper mantle are relatively low (2–3 %) and they do not really lead to considerable non-linear effect. Second, the amplitudes derived from the inversion of the ISC data are usually lower than expected in the nature because of the large damping which should be applied to rid off the noise related instability. In this case, even if we iteratively trace the rays in 3-D, they might appear not significantly closer to the true paths

SED
4, 823–850, 2012

than the 1-D based rays. Third, the linear approach is fast, and it gives us a possibility for performing many trials based on real and synthetic data. This allows us performing thorough selection of free inversion parameters which would be hard in the case of a single non-linear inversion.

In this study, the tomographic inversion is performed separately in three overlapping circular windows with the radius of 10°, covering the study area. For the IBM arc we use the travel times from the revised ISC catalogue which mostly correspond to events located in the study region which were recorded by worldwide stations at all possible epicentral distances. The opposite scheme, with stations in the target area recording the teleseismic events, is almost not used in this case, because of lack of station networks in the study region. The total amount of used rays for the entire region is more than 2 million. The amount of P-data is about ten times larger than that of the S-data. Note that using this ray configuration does not allow obtaining high resolution in tomography reconstruction for the shallowmost sections (above ~50 km depth) where the ray coverage is poor and there is a strong trade-off between velocity and source parameters.

For the inversion, the 3-D velocity distribution is parameterized with a set of nodes which are distributed in 15 depth levels (50, 100, 150, 220, 290, 360, 430, 500, 570, 650, 710, 800, 900, 1000, 1300 km). In each level, the nodes are installed according to the ray coverage; no nodes are set in areas with insufficient data amount. To minimize any artifacts related to grid configuration, the velocity models are calculated independently for the four differently oriented grids with basic orientations at 0°, 22°, 45° and 67° and then averaged. The inversion was performed simultaneously for P- and S-velocity anomalies and for the source parameters (coordinates and origin times). The damping coefficients and weighting of different parameters were estimated based on results of synthetic modeling. The inversion of the matrix is performed using the LSQR algorithm (Paige and Saunders, 1982; Van der Sluis and Van der Vorst, 1987). The main model was obtained by combining 12 separate inversion results (4 models in each of the three circular areas).

SED
4, 823–850, 2012

3 Slab-related seismicity

Unlike the traditional way of presentation of the Benioff seismicity across subduction zones, in Fig. 2 we show the distribution of seismicity from the revised ISC catalogue projected to the vertical profile along the IBM arc. The map view of the profile location and the band, from which the events were considered, is shown in Fig. 2a. The projection of the events to the profile was performed in each zone along the lines with proportional angles in respect to the orientations of opposite sides of the trapezium. We present both the individual events with magnitude indications (Fig. 2b) and the integral released energy in cells 50 × 50 km (Fig. 2c).

Plots in Fig. 2 display some important features which can be used for geodynamic interpretation. The paradox conclusion which can be drawn from this representation of the seismicity distribution is that the events located below 200 km depth beneath the IBM arc form rather vertically oriented clusters than horizontal ones. This seems to contradict a point of view that seismicity in the slab reflects phase transitions which occur at certain depth. So we would rather expect horizontal clusters around 100 km, 200 km and other depth levels where the material of the slab is transformed. They can be seen locally, but less prominently than thin vertical zones of seismicity. The most clear are vertical clusters of seismicity around the distances of 700, 1380 and 1910 km. The later cluster can be represented by a thin vertical "column" of about 700 km high and only ~ 100–200 km width. This cluster corresponds to the Mariana segment which manifests the seismicity at all depths along a relatively narrow vertical band.

Another striking feature is a large seismicity cluster related to the lower part of the northern segment of the Izu-Bonin plate. Between 0 and 900 km along the profile, it tends dipping from 200 km to 300 km depth for the upper boundary of the cluster, and from 400 km to 500 km for the lower boundary. The southern limit of this body roughly fit to the vertical cluster at ~ 700 km distance. In this body, as well as in other places of the section, some events seem to form local linear structures which may represent the orientations of the deformation axes in the slab.

SED
4, 823–850, 2012

These observations possibly indicate that along the profile there are at least four separate segments of the subducting plate which may behave differently. The first northern segment of the Izu-Bonin plate is represented by gently dipping plate with very active seismicity in the depth interval between 300 and 500 km. The next two segments of the Izu-Bonin arc are limited by vertical clusters at 700 km, 1379 km and 1912 km. Unlike the first segment, for these two segments, no significant deep seismicity is observed. The cluster in the middle at 1379 km is observed down to about 350 km depth, which may imply that these two segments are only separated in the upper part and united in the lower part. The southernmost segment corresponds to the Mariana plate. Most of seismicity in the Mariana segment is concentrated in a relatively narrow zone around the mark at 1912 km. Away of this cluster, the Mariana Plate demonstrates very minor deep seismicity with decreasing depths (from 500 km to 200 km) when moving southward.

4 Results of tomographic inversion and verification

The derived models of seismic P- and S-anomalies are shown in seven horizontal sections (Fig. 3) and in 9 vertical sections for Izu-Bonin-Mariana arc (Fig. 4). The areas, where the distance to the nearest grid node is more than 80 km, are shaded; in these areas the data coverage is not sufficient for the tomographic inversion. The variance reduction after the inversion was more than 50 % which shows relatively high level of coherent signal.

The major feature which is clearly seen in horizontal and vertical sections is a slab-related high-velocity anomaly which is observed beneath the entire arc, except for the shallowmost part in the Mariana region where the resolution is poor. This anomaly is generally consistent in P- and S-model, although the amount of the S-data was about ten times smaller than that of P. The correlation of the P- and S-models is an informal argument for the reliability model; on regional scale, the major geological structures, such

SED
4, 823–850, 2012

as subduction, usually affect similarly the P- and S-velocities. Note that this anomaly fits to the deep seismicity distribution in the Benioff zone.

Observing the vertical and horizontal sections helps to determine the shape of the subducting slab. In vertical Sect. 1 we observe the northernmost part of the Izu-Bonin arc. The amount and the quality of data in this area is maximal; therefore the image seems to be well resolved. In this section, the shape of the slab is well repeated in P- and S-anomalies, excluding some features in deepest parts. The recovered slab-related anomaly fits to the distribution of deep seismicity. Here the slab gently dips with the angle of about 35°. For Sect. 2, the slab becomes steeper, but in the transition zone between 400 and 600 km depth it turns to be horizontal. In this section, an enigmatic feature is a prominent positive anomaly in the lower mantle which is clearly seen in both P- and S-models, though with different shapes. Note that in the neighboring sections 1 and 3, this anomaly is not observed. In Sects. 3 and 4, the dipping part of the slab becomes steeper and reaches the angle of 60–70°. The horizontal part of the slab above the transition zone is still observed here. In Sect. 5 the dipping part of the slab disappears, and in the map view we see that the section passes through the gap area between the Izu-Bonin and Mariana plates. In Sects. 7 and 8 we observe the bright images of the Mariana slab which deepens almost vertically. Based on these results, we cannot say definitively if the slab penetrates to the lower mantle or not. In Sect. 8, the slab seems to stop at 700 km depth, whereas in Sect. 7 for P- and S-anomalies we observe high-velocity anomaly below 700 km depth.

The derived model generally agrees with other previously published regional models (Bijwaard et al., 1998; Widiyantoro, 1999; Widiyantoro and van der Hilst, 1996; Gorbatov et al., 2003; Miller et al., 2004, 2005, 2006). Detailed description of comparison of our results with other models is given in discussion chapter.

SED
4, 823–850, 2012

5 Verification

As mentioned previously, the data of ISC catalogue are very noisy. Despite the efforts on pre-processing the data and rejection of outliers, we should confess that noise is still important and it can significantly affect the inversion. To estimate the influence of random noise upon the inversion results, we performed the "odd/even" test which consists in independent inversions of two equal subsets of data (e.g. with odd and even numbers of events) using the same inversion parameters as in the case of the entire dataset. If noise effect is significant, it would generate random anomalies which would be different in two independent results; they should be ignored or smoothed by increasing the damping. The results of this test shown in Fig. 5 demonstrate fairly high consistency of the main patterns which confirm their independence of random noise in the data.

To evaluate the spatial resolution of the model, we have performed the synthetic checkerboard test. The synthetic model was defined as alternating positive and negative rectangular anomalies. For the P-model the horizontal size of the cell was $1 \times 1^{\circ}$ with an empty space of 0.5°; for the S-model the corresponding parameters were $2 \times 1.5^{\circ}$ and 1°. With the depth, the sign of anomalies alternated at every 200 km. To produce the synthetic dataset, we used same rays as in the case of real data inversion. The synthetic times were perturbed with random noise with the statistical distribution which was estimated after analysis of real residuals in the revised ISC catalogue. The magnitude of the noise was 0.5 s and 0.8 s for the P- and S-data, respectively, which leaded to the same variance reduction after inversion (about 50 %) as in the real data case. When reconstructing the synthetic model, the values of the inversion parameters were the same as in the case of real data inversion. Figure 6 displays the reconstruction of the checkerboard model at different depths. It shows that in the central part of the area, where the slab is located, the resolution is fair. However, below 700 km depth the resolution becomes poorer and does not allow recovering such small-scale features.

SED
4, 823–850, 2012

An important test consists in reconstruction of a synthetic model with realistic configuration of anomalies. In Fig. 7 we present a model which reproduces the configuration of the slab in horizontal and vertical sections. The anomalies were defined as free-shaped anomalies along the vertical sections and had the fixed shape in the direction across the section within a certain band. This method allows defining the realistic shapes of different segments of the slab. In this model, the Izu-Bonin slab is gently dipping and becomes horizontal in the transition zone. On the contrary, The Mariana slab consists of three segments and almost vertically dips down to 1200 km. Between the Mariana and Izu-Bonin arcs we define a small gap. As in the case of the checkerboard test, the synthetic data were perturbed with random noise of 0.5 and 0.8 s magnitude for P- and S-data, respectively. The results of the reconstruction in horizontal and vertical sections show that the main patterns in the mantle are correctly reconstructed. However, the uppermost structures in the Mariana area are strongly biased because of lack of data and trade-off between velocity structures and source parameters. In the lower mantle, the slab-related anomaly is strongly smeared, especially for the S-model, however it is retrieved at a correct place.

6 Discussion

The main feature of the obtained model is the slab-related high-velocity anomaly which is clearly observed in all horizontal sections of P- and S-model, except for the uppermost part where it is not resolved for the Mariana area. In vertical sections we observe complex behavior of the subducting plate which changes the shape along the IBM arc. Based on these results we propose a scenario explaining the present shape of the slab which is schematically shown in Fig. 10.

According to (Seno and Maruyama, 1984; Seno et al., 1993; Hall et al., 1995a, b; Hall, 2002), presently curved shape of the IBM trench (violet line in Fig. 8) was much straighter in the recent past (e.g. 12 Ma) as schematically shown with black line in left plot in Fig. 8. An indirect argument for this hypothesis is the nearly linear distribution of

SED
4, 823–850, 2012

high-velocity anomalies at 975 km depth shown in Fig. 8 which probably represent the curvature of the trench in the past (dotted line). It can be seen that since that time, there were both backward and forward displacements of the trench in different segments. Note that a segment with the forward displacement corresponds to the presence of the Ogasawara large igneous plateau. The change of the subduction shape roughly corresponds to transitions between different displacement regimes of the trench. Based on the results of tomographic inversion we propose our back-time reconstruction to about 10–12 Ma. In sections to the left of Fig. 8, which roughly correspond to vertical sections 1, 2, 3 and 8 in Fig. 4, we present the hypothetical evolution of subduction in different segments of IBM arc. We propose that initially the subduction occurred along a weakly curved trench and the shape of the slab was generally similar throughout the IBM arc (namely with the dipping angles of 40–50 degrees).

For Sects. A1–A2 we expect a considerable backward displacement of the trench. In this section the oceanic lithosphere seems to be united with a large segment beneath Japan where the slab is relatively shallow and turns to be horizontal in the transition zone to a large extent (Zhao et al., 2009). The reason why this old and dense lithosphere beneath Japan behaves in this way, is actively discussed in the literature (e.g. Zhao et al., 2009). It might be due to "roof" shape of the slab which gives additional straight and prevents steep bending of the plate. The horizontal segment observed in Sects. A1–A2 might be united with this large body in the transition zone beneath Japan which is moving to the western direction with a constant rate. Moving back of the trench in this area causes decreasing the dipping angle of the slab, as shown in Sects. A1–A2 in Fig. 8.

For Sects. B1–B2, the situation seems to be significantly different. Here the shallow part of the slab seems to be detached from the horizontal body in the transition zone. In this part of the arc the trench remains at the same position. The continued subduction at a rate of about 4 cm yr^{-1} (DeMets et al., 2010) causes accumulation of the slab material in the transition zone (stage 2). When reaching a critical volume, the accumulated denser material starts to descend to the lower mantle.

SED
4, 823–850, 2012

In Sects. C1–C2 we observe steepening of the slab. In this segment of the arc the trench is though to migrate forward which is possibly caused by the presence of the large igneous Ogasawara Plateau. It is possible that this plateau increased the strength of the lithosphere and made it more buoyant. That is why, when this plateau reached the trench, it stopped the subduction and leaded to displacement of the trench along the incoming plate movement. In this case, the anchored lower part was fixed, and the displacement of the upper part caused the steepening of the slab.

The last Sects. D1–D2 corresponds to the vertical Sect. 8 (Fig. 4) which passes across the Mariana segment. According to Miller et al. (2006b) and authors referred therein, the Mariana trench is moving backward, and initially the situation was similar to Sects. A1–A2. The Mariana plate was detached from the Isu-Bonin plate by the Ogasawara plateau which served as a "knife" which cut the lithosphere. We propose that this detachment was facilitated by remnant heat which may be kept in plume traces beneath the plateau. The isolated heavy Mariana plate cannot behave as the northernmost part of the Izu-Bonin plate which is supported by the Japanese shallow slab. Even if in stage 1 the subduction had a normal dipping angle (e.g. 45°), in stage 2, the shallow part of the slab had to be detached from the deep one, and a new subduction zone originated. The newly formed subduction is mostly driven by high density of the subducted lithosphere which pulls it down. In this case, it behaves not as a normal subduction: the descending of the plate occurs due to both ocean plate movement and trench displacement, as shown in Sects. D1–D2. This is supported by relatively slow rate of the subduction ($\sim 2\,\mathrm{cm\,yr^{-1}}$) and an approximately same rate of the slab retreat in the Mariana trench (DeMets, 2010). The remnant part of the previous subduction zone could descend to the transition zone and then further continued sinking to the lower mantle. A possible location of sinking of the older subducted slab is in the area, where the resolution of the tomographic model is poor. However, a strongly smeared anomaly of high P-velocity model in the lower mantle can be interpreted as a trace of the previous subduction and it would fit to this hypothesis.

SED
4, 823–850, 2012

The variability of the subduction regimes leaded to clear segmentation of the IBM subduction zone with the boundaries marked with vertical seismicity clusters (Fig. 2). Similarly as in Miller et al. (2006a), between the Mariana and Izu-Bonin segments we can see the gap corresponding to vertical Sect. 5 in Fig. 4 which is observed down to 400 km depth. Initially it was formed by the effect of the Ogasawara plateau. Further opening of this gap occurred due oblique orientation of the Pacific Plate movement in respect to the northern part of the Mariana loop. The strike-slip displacement along the trench in this area causes the further detachment of the upper part of the slab. The lower part of the slab seems to be united and it probably corresponds to the stage when the trench was not perturbed by forward and backward displacements.

7 Conclusions

The main result of this study is the new model of seismic velocity heterogeneities of P- and S-waves in the mantle beneath the Izu-Bonin and Mariana arcs which was constructed from tomographic inversion of global travel time data (ISC). This model was thoroughly verified using a series of different tests which showed generally high robustness of the results. The main feature of this result is a slab-related anomaly which is similarly expressed in the P- and S-models. There is a general correlation with previous results derived by other authors; however in details we have detected some new features. We have found that the slab beneath IBM arc has strongly variable dipping angle which generally correspond to the loops of the trench shape. We also analyze the distribution of the deep seismicity which was projected to the profile along the trench. The striking feature of the seismicity distribution is that deep seismic events form clear vertical clusters which generally fit to the limits of the IBM arc segments. We propose that these clusters mark the boundaries between autonomous parts of the slab which may subduct independently with different rates. We propose the scenario which explains the variable dipping angle of the slab beneath the IBM arc. In the northernmost part of the Izu-Bonin zone, the lithosphere is relatively young and buoyant. This and

SED
4, 823–850, 2012

also the trench retreat can explain a gentle deepening of the slab to the angle of about 35 degrees. In the southern segment of the Izu-Bonin arc, the slab is nearly vertical which can be explained by forward displacement of the trench. In the Mariana segment, despite of backward migration of the arc, the slab remains nearly vertical. This can only be explained by jumping the subduction zone from one place to another. Between the Mariana and Izu-Bonin subduction zone we observe a clear gap in the slab which is detected down to about 400 km depth.

This model can be used for thermo-mechanical modeling of the subduction processes, as well as for other implications in geological and geophysical studies.

Acknowledgements. This study is supported by the Multidisciplinary project of the SB RAS No. 20 and the Project ONZ RAS No. 7.3.

References

Baker, E. T., Embley, R. W., Walker, S. L., Resing, J. A., Lupton, J. E., Nakamura, K.-I., de Rode, C. E. J., and Massoth, G. J. : Hydrothermal activity and volcano distribution along the Mariana arc, J. Geophys. Res., 113, B08S09, doi:10.1029/2007JB005423, 2008.

Bassin, C., Laske, G., and Masters, G.: The current limits of resolution for surface wave tomography in North America, EOS, Trans. Am. Geophys. Un., 81, F897, 2000.

Hilde, T. W. C. and Uyeda, S. (Eds.): Geodynamics of the Western Pacific-Indonesian Region, Geodyn. Ser., AGU, Washington, D. C., 11, 287–301, 457 pp., doi:10.1029/GD011, 1983.

Bijwaard, H., Spakman, W., and Engdahl, E. R.: Closing the gap between regional and global travel time tomography, J. Geophys. Res., 103, 30055–30078, 1998.

Crawford, A. J., Beccaluva, L., and Serri, G.: Tectono-magmatic evolution of the West Philippine – Mariana region and the origin of boninites, Earth Planet. Sci. Lett., 54, 346–356, 1981.

DeMets, C., Gordon, R. G., Argus, D. D., and Stein, S.: Effect of recent revisions to the geomagnetic reversal time scale on estimates of current plate motions, Geophys. Res. Lett., 21, 2191–2194, doi:10.1029/94GL02118, 1994.

DeMets, C., Gordon, R. G., and Argus, D. F.: Geologically current plate motions, Geophys. J. Int., 181, 1–80, 2010.

SED

4, 823–850, 2012

Dobretsov, N. L., Koulakov, I., and Litasov, Y.: Fluid and magma migration paths and composition of volcanic rocks of Kamchatka, Russ. Geol. Geoph., 12, (in press) 2012.
Engdahl, E. R., van der Hilst, R. D., and Buland, R.: Global teleseismic earthquake relocation with improved travel times and procedures for depth determination, B. Seismol. Soc. Am., 88, 722–743, 1998.
Gorbatov, A. and Kennett, B. L. N.: Joint bulk-sound and shear tomography for western Pacific subduction zones, Earth Planet. Sci. Lett. 210, 527–543, 2003.
Hall, R.: Cenozoic geological and plate tectonic evolution of SE Asia and the SW Pacific: Computer-based reconstructions, model and animations, J. Asian Earth Sci., 20, 353–431, 2002.
Hall, R., Ali, J. R., Anderson, C. D., and Baker, S. J.: Origin and motion history of the Philippine Sea Plate, Tectonophysics, 251, 229–250, 1995a.
Hall, R., Fuller, M., Ali, J. R., and Anderson, C. D. : The Philippine Sea Plate: Magnetism and reconstructions, in Active Margins and Marginal Basins of the Western Pacific, Geophys. Monogr. Ser., 88, edited by: Taylor, B. and Netland, J., AGU, Washington D. C., 371–404, 1995b.
Katsumata, M. and Sykes, L. R.: Seismicity and tectonics of the western Pacific: Izu-Mariana-Caroline and Ryukyu-Taiwan regions, J. Geophys. Res., 74, 5923–5948, doi:10.1029/JB074i025p05923, 1969.
Kelemen, P. B., Hanghoi, K., and Greene, A. R.: One view of the geochemistry of subduction-related magmatic arcs, with an emphasis on primitive andesite and lower crust, in: The Crust, edited by: Holland, H., Turekian, K., and Rudnick, R. L., Treatise on Geochemistry, 3, Elsevier-Pergamon, Oxford, 593–659, 2004.
Kennett, B. L. N., Engdahl, E. R., and Buland, B.: Constraints on seismic velocities in the Earth from travel times, Geophys. J. Int., 122, 108–124, 1995.
Koulakov I.: LOTOS code for local earthquake tomographic inversion. Benchmarks for testing tomographic algorithms, B. Seismol. Soc. Am., 99, 194–214, doi:10.1785/0120080013, 2009.
Koulakov, I.: High-frequency P and S velocity anomalies in the upper mantle beneath Asia from inversion of worldwide traveltime data, J. Geophys. Res., 116, B04301, doi:10.1029/2010JB007938, 2011.
Koulakov, I. and Sobolev, S. V.: Tomographic Image of Indian Lithosphere Break-off beneath the Pamir Hindukush Region, Geophys. J. Int., 164, 425–440, 2006.

SED
4, 823–850, 2012

Koulakov, I., Tychkov, S., Bushenkova, N., and Vasilevskiy, A.: Structure and dynamics of the upper mantle beneath the Alpine-Himalayan orogenic belt from teleseismic tomography, Tectonophysics, 358, 77–96, 2002.

Koulakov, I., Kaban, M. K., Tesauro, M., and Cloetingh, S.: P and S velocity anomalies in the upper mantle beneath Europe from tomographic inversion of ISC data, Geophys. J. Int., 179, 345–366, doi:10.1111/j.1365-246X.2009.04279.x, 2009.

Miller, M. S., Gorbatov, A., and Kennett, B. L.: Heterogeneity within the subducting Pacific slab beneath the Izu-Bonin-Mariana arc: Evidence from tomography using 3D ray tracing inversion techniques, Earth Planet. Sci. Lett., 235, 331–342, 2005.

Miller, M. S., Gorbatov, A., and Kennet, B. L. N.: Three-dimensional visualization of a near vertical slab tear beneath the southern Mariana arc, Geochem. Geophys. Geosyst., 7, Q06012, doi:10.1029/2005GC001110, 2006a.

Miller, M. S., Kennett, B. L. N., and Toy, V. G.: Spatial and temporal evolution of the subducting Pacific plate structure along the western Pacific margin, J. Geophys. Res., 111, B02401, doi:10.1029/2005JB003705, 2006b.

Miller, M. S., Kennett, B. L., and Lister, G. S.: Imaging changes in morphology, geometry, and physical properties of the subducting Pacific plate along the Izu-Bonin-Mariana arc, Earth Planet. Sci. Lett., 224, 363–370, 2011.

Müller, R. D., Roest, W. R., Royer, J. Y., Gahagan, L. M., and Sclater, J. G.: Digital isochrons of the World's ocean floor, J. Geophys. Res., 102, 3211–3214, doi:10.1029/96JB01781, 1997.

Paige, C. C. and Saunders, M. A.: LSQR: An algorithm for sparse linear equations and sparse least squares, ACM Trans. Math. Soft., 8, 43–71, 1982.

Peive, A. V., (Ed.): Geology of the Philippine Sea floor, "Nauka", Moscow, p. 261, 1980.

Petersen, J.: Der Boninit von Peel Island, Jahrb Hamburg, Wiss Anst, 8, 341–349, 1891.

Seno, T. and Maruyama, S.: Paleogeographic reconstruction and origin of the Philippine Sea, Tectonophysics, 102, 53–84, 1984.

Seno, T., Stein, S., and Gripp, A. E.: A model for the motion of the Philippine Sea Plate consistent with NUVEL-1 and geological data, J. Geophys. Res., 98, 17941–17948, 1993.

Van der Hilst, R. D. and Seno, T.: Effects of relative plate motion on the deep structure and penetration depth of slabs below the Izu-Bonin and Mariana island arcs, Earth Planet. Sci. Lett., 120, 375–407, 1993.

Van der Hilst, R. D., Engdahl, E. R., Spakman, W., and Nolet, G.: Tomographic imaging of subducted lithosphere below northwest Pacific island arcs, Nature, 353, 37–42, 1991.

SED
4, 823–850, 2012

Van der Sluis, A. and Van der Vorst, H. A.: Numerical solution of large, sparse linear algebraic systems arising from tomographic problems, in: Seismic tomography, edited by: Nolet, G., Reidel, Dortrecht, 49–83, 1987.

Widiyantoro, S. and Van der Hilst, R. D. : Structure and evolution of lithospheric slab beneath the Sunda Arc, Indonesia, Science, 271, 1566–1570, 1996.

Widiyantoro, S., Kennett, B. L. N., and Van der Hilst, R. D.: Seismic tomography with P and S data reveals lateral variations in the rigidity of slabs, Earth Planet. Sci. Lett., 173, 91–100, 1999.

Zhao, D., Tian, Y., Lei, J., Liu, L., Zheng, S.: Seismic image and origin of the Changbai intraplate volcano in East Asia: Role of big mantle wedge above the stagnant Pacific slab, Phys. Earth Planet. Inter., 173, 197–206, 2009.

SED

4, 823–850, 2012

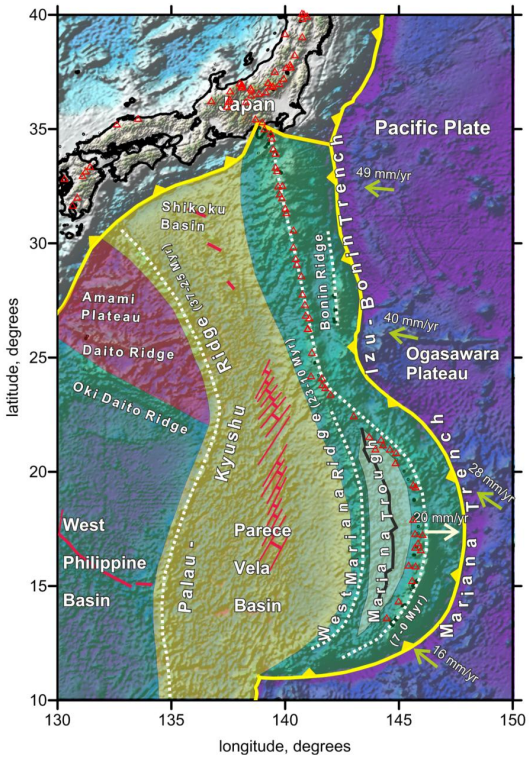

Fig. 1. The main geographic and tectonic units of the studied region. Background is map of topography/bathymetry. The colors indicate the regions of the oceanic crust of different ages: Pre-Cretaceous (green), Pre-Mesozoic (red), Pre-Miocene (yellow), Pre-Quaternary age (white), sea floor of Pacific Ocean, Pre-Triassic (blue). White dotted lines depict arcs (ancient and present). Names and ages of arcs are indicated. Arrows with numbers present the displacement rates in respect to Philippine plate (DeMets et al., 2010). The red triangles indicate active volcanoes (including submarine and hydrothermal volcanoes).

SED
4, 823–850, 2012

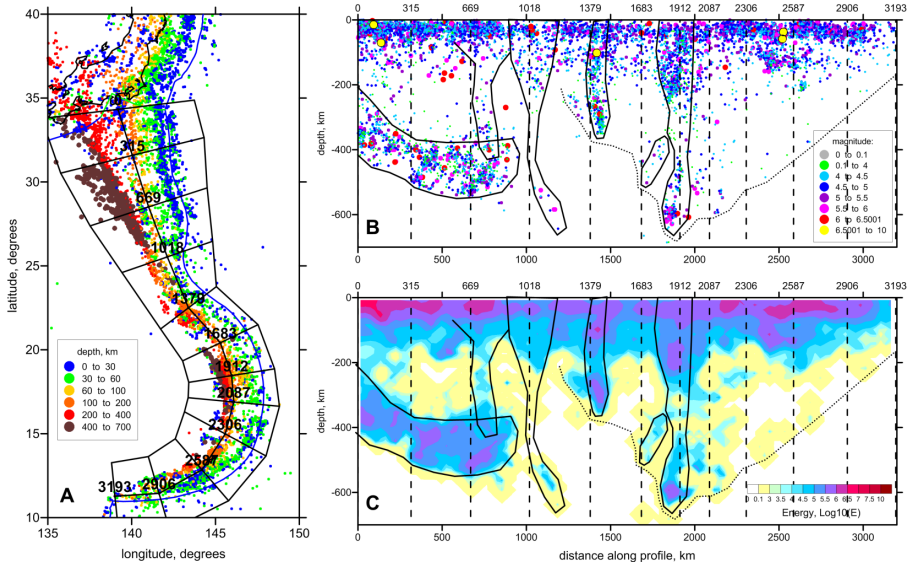

Fig. 2. (A) Distribution of earthquakes in map view. Colored dots depict earthquake hypocenters. Segments indicate the area in which the seismicity was considered. Line in the center of the segments is the location of vertical profile for plots **(B)** and **(C)**. **(B)** The distribution of earthquakes in the vertical cross section along the arc; colors and sizes of dots indicate the magnitude of events. **(C)** Total seismic energy release along the same vertical section in 50 × 50 km cells. Black lines in **(B)** and **(C)** highlight the cluster of earthquakes discussed in the text. Dotted line depicts the bottom of the seismogenic zone beneath the Mariana Arc.

SED
4, 823–850, 2012

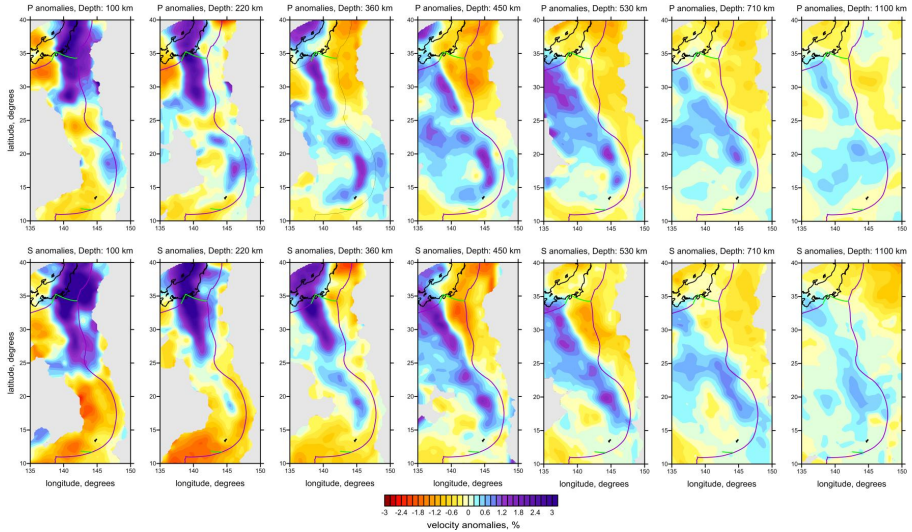

Fig. 3. The results of the real data inversion. The distribution of the P- and S-anomalies are shown at different depths. Purple line indicates tectonic boundaries according to Fig. 1.

SED
4, 823–850, 2012

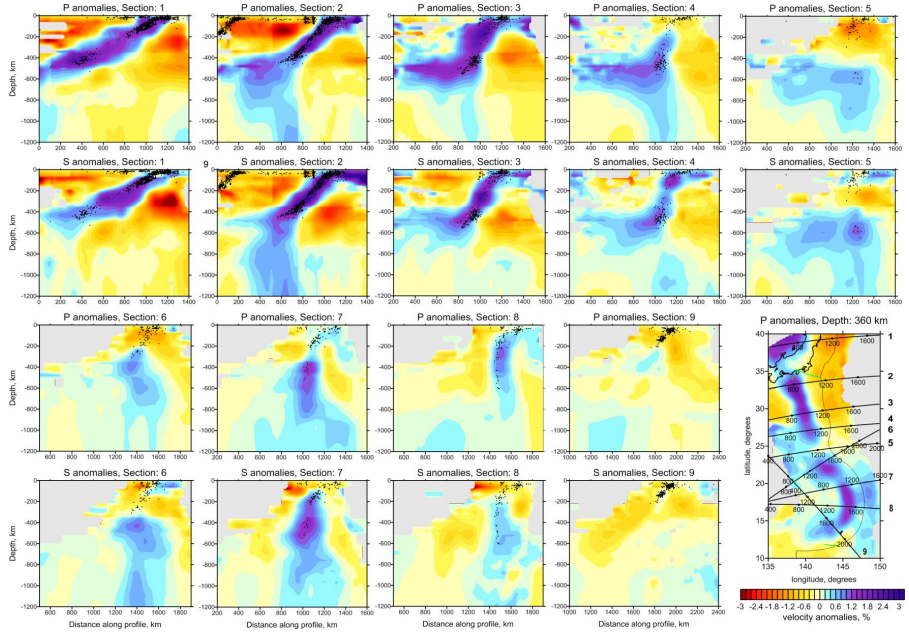

Fig. 4. The results of real data inversion. P- and S-anomalies are presented in vertical cross sections across the Izu-Bonin-Mariana arc; locations of sections are shown in the map in the lower right corner. Black dots are the earthquake hypocenters located at a distance of no more than 50 km from the profile.

SED
4, 823–850, 2012

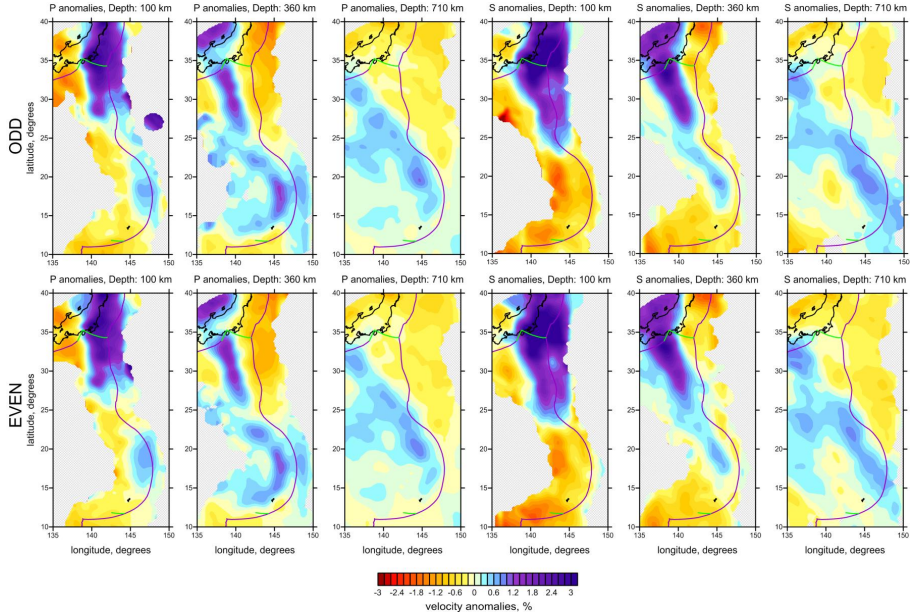

Fig. 5. Test with even and odd numbers of sources to estimate the level of random noise. The distribution of P- and S-anomalies are shown at different depths. The upper and lower rows correspond to results with odd and even numbers of sources, respectively.

SED
4, 823–850, 2012

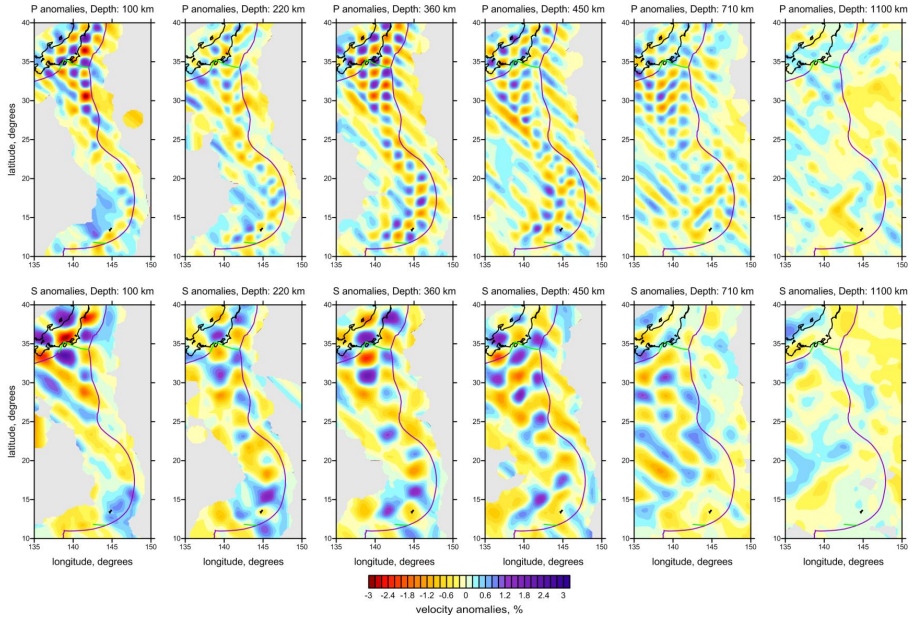

Fig. 6. Synthetic test "Checkerboar". The distribution of P- and S-anomalies are shown at different depths. The sizes of synthetic anomalies are: $1^\circ \times 1^\circ$ for the P-model with the distance between the anomalies of 0.5° and $2^\circ \times 1.5^\circ$ for S-model with the distance between the anomalies of 1°.

SED
4, 823–850, 2012

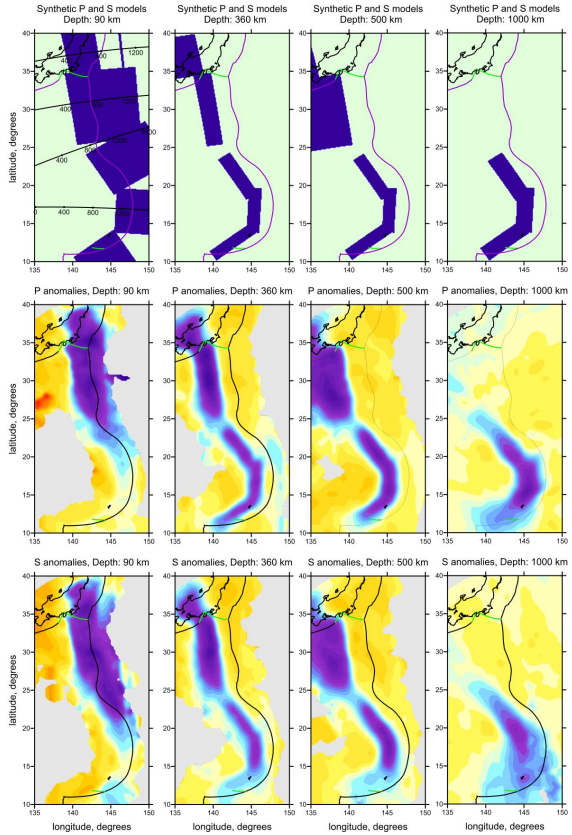

Fig. 7. Synthetic tests with slab-shaped anomalies. The results of inversion are shown in horizontal and vertical sections. Locations of the profiles are shown in map corresponding to the model definition at 90 km depth.

SED
4, 823–850, 2012

Segmentation of the Izu-Bonin and Mariana plates

K. Jaxybulatov et al.

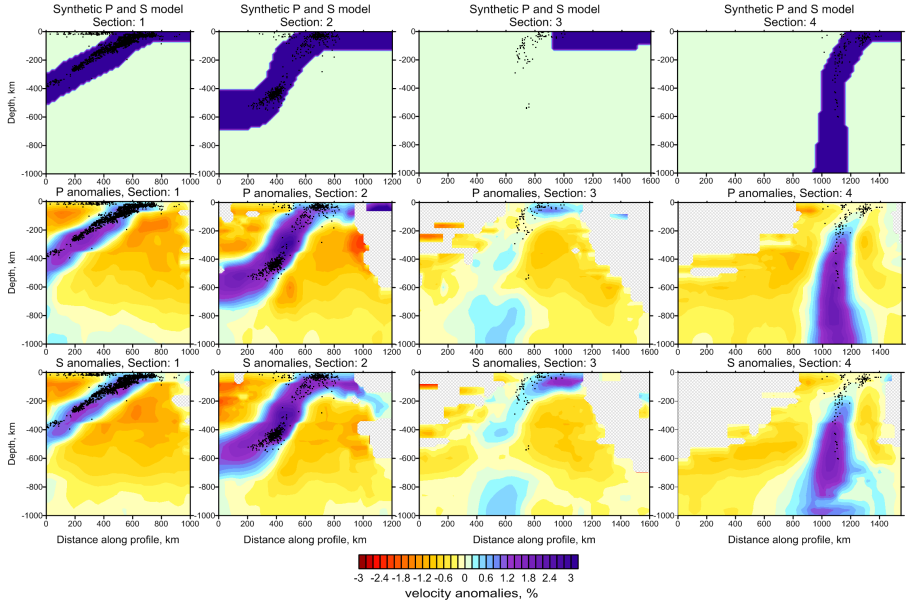

Fig. 7. Continued.

SED
4, 823–850, 2012

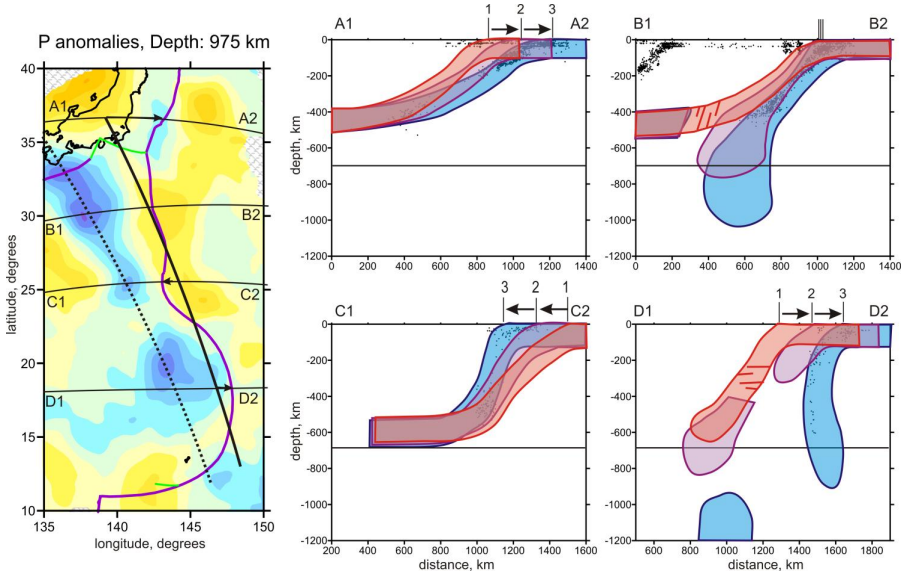

Fig. 8. Reconstruction of the subduction evolution in different segments of the Izu-Bonin and Mariana arcs. Left: map view of the area. Violet line is the present location of the arc; black line is a possible location of the arc about 12 Ma; dotted line is a possible location of the slab material at about 1000 km depth, background is P-velocity anomalies at 975 km depth; location of profiles for schematic representation are shown. Right: different regimes of subduction in four different segments of the arc. Color of patterns corresponds to the age: red is ~12 Ma, violet is ~6 Ma and blue is present. Bars with nimbers 1, 2 and 3 correspond to the location of the trench in the three episodes. Black dots depict the present seismicity around the corresponding segment; solid line is the boundary between the upper and lower mantle.

SED
4, 823–850, 2012